

Metabolomics for the identification of early biomarkers of cisplatin-induced nephrotoxicity in a mouse model of cisplatin-induced acute kidney injury

Yong Lim¹, Nicholas Tonial¹, Emily Hartjes¹, Aaron Haig², Thomas Velenosi³, and Bradley Urquhart¹

¹University of Western Ontario

²London Health Sciences Centre University Hospital

³The University of British Columbia

November 30, 2022

Abstract

Background and Purpose: Cisplatin-induced nephrotoxicity manifests as acute kidney injury (AKI) in approximately one third of patients receiving cisplatin therapy. Current measures of AKI are inadequate in detecting AKI prior to significant renal injury, and better biomarkers are needed for early diagnosis of cisplatin-induced AKI. **Experimental Approach:** C57BL/6 and FVB/N mice were treated with a single intraperitoneal injection of cisplatin (15 mg kg⁻¹) or saline. Plasma, urine, and kidney samples were collected prior to cisplatin injection and 24-, 48-, 72-, and 96-hours following cisplatin injection. Untargeted metabolomics was employed using liquid chromatography-mass spectrometry to identify early diagnostic biomarkers for cisplatin-induced AKI. **Key Results:** There was clear metabolic discrimination between saline and cisplatin-treated mice at all timepoints (day 1 to day 4). In total, 26 plasma, urine, and kidney metabolites were identified as exhibiting early alterations following cisplatin treatment. Several of the metabolites showing early alterations were associated with mitochondrial function and energetics, including intermediates of the tricarboxylic acid cycle, regulators of mitochondrial function and indicators of fatty acid β -oxidation dysfunction. Furthermore, several metabolites were derived from the gut microbiome. **Conclusion and Implications:** Our results highlight the detrimental effects of cisplatin on mitochondrial function and demonstrate potential involvement of the gut microbiome in the pathophysiology of cisplatin-induced AKI. Here we provide a panel of metabolites to guide future clinical studies of cisplatin-induced AKI and provide insight into potential mechanisms behind cisplatin nephrotoxicity.

TITLE: Metabolomics for the identification of early biomarkers of cisplatin-induced nephrotoxicity in a mouse model of cisplatin-induced acute kidney injury

Running Title: Metabolomics of cisplatin nephrotoxicity

AUTHORS

Yong Jin Lim¹(ylim33@uwo.ca)

Nicholas C. Tonial¹(ntonial2025@meds.uwo.ca)

Emily D. Hartjes¹(ehartjes@uwo.ca)

Aaron Haig²(aaron.haig@lhsc.on.ca)

Thomas J. Velenosi³(thomas.velenosi@ubc.ca)

Bradley L. Urquhart^{1,4}(Brad.Urquhart@schulich.uwo.ca)

AFFILIATIONS

¹Department of Physiology and Pharmacology, Schulich School of Medicine and Dentistry, Western University, London, ON, Canada

²Department of Pathology and Laboratory Medicine, Schulich School of Medicine & Dentistry, Western University, London, ON, Canada

³Faculty of Pharmaceutical Sciences, University of British Columbia, Vancouver, BC, Canada

⁴Division of Nephrology, Department of Medicine, Schulich School of Medicine & Dentistry, Western University, London, ON, Canada

CORRESPONDENCE

Bradley L. Urquhart, PhD

1151 Richmond Street

Medical Sciences Building Room 216

London, ON, N6A 5C1

E-mail: Brad.Urquhart@schulich.uwo.ca

Phone: (519) 661-3756

Fax: (519) 661-3827

Word Count: 3839 (introduction, results, discussion, conclusion)

BULLET POINT SUMMARY

What is already known:

Cisplatin causes nephrotoxicity, which manifests as acute kidney injury (AKI) in approximately one-third of patients

Serum creatinine is a poor diagnostic biomarker of kidney injury

What this study adds:

26 plasma, urine, and kidney metabolites were identified to exhibit early alterations following cisplatin administration

Many of the identified metabolites were associated with mitochondrial dysfunction or were gut-derived

Clinical Significance:

A large panel of metabolites were identified for future clinical studies of early detection of AKI

Metabolite changes provide potential therapeutic targets for nephroprotective interventions

ABSTRACT

Background and Purpose: Cisplatin-induced nephrotoxicity manifests as acute kidney injury (AKI) in approximately one third of patients receiving cisplatin therapy. Current measures of AKI are inadequate in detecting AKI prior to significant renal injury, and better biomarkers are needed for early diagnosis of cisplatin-induced AKI.

Experimental Approach: C57BL/6 and FVB/N mice were treated with a single intraperitoneal injection of cisplatin (15 mg kg⁻¹) or saline. Plasma, urine, and kidney samples were collected prior to cisplatin injection and 24-, 48-, 72-, and 96-hours following cisplatin injection. Untargeted metabolomics was employed

using liquid chromatography-mass spectrometry to identify early diagnostic biomarkers for cisplatin-induced AKI.

Key Results: There was clear metabolic discrimination between saline and cisplatin-treated mice at all timepoints (day 1 to day 4). In total, 26 plasma, urine, and kidney metabolites were identified as exhibiting early alterations following cisplatin treatment. Several of the metabolites showing early alterations were associated with mitochondrial function and energetics, including intermediates of the tricarboxylic acid cycle, regulators of mitochondrial function and indicators of fatty acid β -oxidation dysfunction. Furthermore, several metabolites were derived from the gut microbiome.

Conclusion and Implications: Our results highlight the detrimental effects of cisplatin on mitochondrial function and demonstrate potential involvement of the gut microbiome in the pathophysiology of cisplatin-induced AKI. Here we provide a panel of metabolites to guide future clinical studies of cisplatin-induced AKI and provide insight into potential mechanisms behind cisplatin nephrotoxicity.

Keywords: Metabolomics, cisplatin, nephrotoxicity, acute kidney injury, biomarkers

1. INTRODUCTION

Cisplatin is a platinum-based chemotherapeutic agent used in the treatment of a wide variety of malignancies . Although cisplatin is highly effective and widely used, clinical usage of cisplatin is often limited by toxicity to non-cancerous tissues. The kidneys are especially sensitive to cisplatin toxicity, and as such, cisplatin-induced nephrotoxicity is the dose-limiting factor in cisplatin therapy . Cisplatin is primarily excreted by the kidneys, through both glomerular filtration and tubular secretion . Transporter-mediated uptake of cisplatin by tubular epithelial cells results in the renal accumulation of cisplatin, subsequent biotransformation into highly reactive thiol metabolites, and ultimately cell injury .

Cisplatin-induced nephrotoxicity manifests as acute kidney injury (AKI) in approximately one-third of patients . AKI is characterised by a rapid decline in kidney function and is associated with increased risk for chronic kidney disease, major cardiovascular events, and mortality . AKI is defined by the Kidney Disease Improving Global Outcomes (KDIGO) as a [?] 1.5-fold increase in serum creatinine (SCr) versus baseline, or as an increase in SCr [?] 26.5 $\mu\text{mol/L}$. Though SCr is used for clinical diagnosis of AKI, detectable changes in SCr only occur after substantial kidney injury and functional impairment . Earlier identification of nephrotoxicity is necessary to initiate nephroprotective interventions for cisplatin-induced AKI. The search for diagnostic/prognostic biomarkers of AKI has yielded the discovery of several serum and urinary protein biomarkers, including neutrophil gelatinase-associated lipocalin, kidney injury molecule-1, cystatin C, tissue inhibitor of metalloproteinase 2, and insulin-like growth factor binding protein 7 . However, these markers are not specific to AKI, nor are they specific for any one etiology of AKI. There is a consensus that the application of a panel of biomarkers is better suited for the early detection of AKI, evaluation of AKI severity/prognosis, and discrimination of AKI etiology, rather than the use of any one single biomarker .

In this study, we aimed to identify early biomarkers of cisplatin-induced AKI through metabolomics analysis of mouse plasma, kidney, and urine samples taken at multiple time points throughout AKI progression from two different strains of mice. We used C57BL/6 and FVB/N mice, with FVB/N mice having been reported to have higher susceptibility to cisplatin-induced AKI compared to C57BL/6 . To date, there have been few studies utilizing metabolomics in rodent models of cisplatin-induced AKI. Investigating metabolic alterations in all three of plasma, urine, and kidney tissue samples at multiple timepoints throughout AKI progression is needed to characterize biomarkers from treatment to establishment of AKI.

2. METHODS

2.1 Materials

Cisplatin (Accord Healthcare, 1 mg/mL) was purchased from University Hospital Pharmacy (London, ON, Canada). Chlorpropamide was purchased from Toronto Research Chemicals (Toronto, ON, Canada), atenolol-d7 from Sigma-Aldrich (Oakville, ON, Canada), flurazepam from Cerilliant (Round Rock, TX,

USA), and DL-2-aminoheptanedioic acid from Bachem (Torrence, CA, USA). HPLC grade acetonitrile was purchased from Millipore Sigma (Oakville, ON, Canada). 10% formalin was purchased from VWR International (Mississauga, ON, Canada).

2.2 Animal model

Wild-type male C57BL/6 and FVB/N mice (8-12 weeks old) were obtained from Charles River Laboratories. All experimental protocols and animal care procedures were conducted in accordance with the Canadian Council on Animal Care and were approved by the Animal Care Committee of Western University. All mice were housed in standard caging with a 12-hour light cycle and were given standard rodent chow and water *ad libitum*. Eight mice from both the FVB/N and C57BL/6 strains were used as baseline controls. Both C57BL/6 and FVB/N mice were randomly divided into “control” and “cisplatin” groups. Cisplatin groups were given a single intraperitoneal injection of cisplatin (15 mg kg⁻¹) and control mice were given an equal volume of 0.9% saline. Mice were euthanized 1, 2, 3, and 4 days after treatment for sample collection. A ketamine/xylazine mixture (100 mg kg⁻¹ and 12.5 mg kg⁻¹, respectively) was used for anesthesia, followed by intracardiac blood collection and bilateral thoracotomy for confirmation of euthanasia. Urine samples and both kidneys were also collected upon euthanasia. Samples were also isolated from untreated C57BL/6 and FVB/N mice to be used as baseline controls. The number of samples collected varied based on sample collection/availability and exact numbers of samples collected for each sample type in each experimental group can be found in **Table S1**.

2.3 Assessment of renal injury

Mouse plasma creatinine levels were measured with ultra performance liquid chromatography coupled with mass spectrometry (UPLC-MS). Ice-cold acetonitrile (ACN) containing 50 µM creatinine-d3 (internal standard) was added to plasma samples for protein precipitation (3:1 ratio). Following the addition of ACN, all samples were vortexed, incubated at -20°C for 20 minutes, and centrifuged at 14000 g for 10 minutes. The resulting supernatant was isolated and used for creatinine quantification. Chromatographic separation was achieved using a Waters ACQUITY UPLC BEH Amide column (1.7 µm particle size, 2.1 mm x 100 mm) maintained at 45°C in a Waters ACQUITY UPLC I-Class system. The mobile phase consisted of A) water + 0.1% formic acid and B) ACN + 0.1% formic acid. Mobile phase flow rate was set to 0.45 mL/min and the following mobile phase gradient was used: 0–0.5 mins, 90% B; 0.5–1 min, 90–60% B; 1–1.5 min, 60% B; 1.5–1.51 min, 60–90%B; 1.51–2.5 min, 90% B. Creatinine was measured in positive electrospray ionization mode using a Waters Xevo G2-S QToF mass spectrometer. The creatinine signal was normalized to the creatinine-d3 internal standard and concentrations were quantified using a creatinine standard curve ranging from 0.78125 – 100 µM creatinine, using TargetLynx version 4.1 software.

Kidney samples were fixed in 10% formalin. All tissue processing, sectioning, and staining were performed by the Department of Pathology and Laboratory Medicine at Western University, Canada. Kidneys were dehydrated, embedded in paraffin, and cut into 5 µm sections using a microtome. Sections were then mounted on slides and subsequently stained with hematoxylin and eosin (H&E). The extent of renal injury was assessed using light microscopy by a trained pathologist who was blinded to the treatment conditions. Tubular injury was graded on an arbitrary scale of 0 – 5 (0, none; 1, <11%; 2, 11% to 25%; 3, 26% to 45%; 4, 46% to 75%; 5, >75%), based on the degree of observed proximal tubule dilation, brush-border damage, proteinaceous casts, interstitial widening, and necrosis.

2.4 Sample preparation for untargeted metabolomics

Ice-cold acetonitrile containing chlorpropamide (4 µM), atenolol-d7 (1.8 µM), flurazepam (0.15 µM) and DL-2-aminoheptanedioic acid (100 µM) as internal standards, was added to plasma and urine samples for protein precipitation (3:1 ratio). Kidney samples (50 mg) were homogenized in 150 µL of ACN containing internal standards. Following the addition of ACN, all samples were vortexed, incubated at -20°C for 20 minutes, and centrifuged at 14000 g for 10 minutes. Supernatant from the protein precipitation was diluted 1 in 5 with water. Diluted samples were transferred into glass vials for UPLC-MS analysis. A pooled sample was generated to serve as quality control throughout the metabolomics run.

2.5 Chromatography and Mass Spectrometry

Chromatography and mass spectrometry instrumentation were the same as described previously in “Assessment of Renal Injury”. 2 μL of sample was injected from each vial. Sample injection order was randomized, and the quality control pooled sample was injected after every 6 sample injections throughout the run. Chromatographic separation was achieved using a Waters ACQUITY UPLC HSS T3 column (1.8 μm particle size, 2.1 mm x 100 mm) maintained at 45°C. The mobile phase consisted of A) water + 0.1% formic acid and B) ACN + 0.1% formic acid. Mobile phase flow rate was set to 0.45 mL min^{-1} and the following mobile phase conditions were used: 0–2 mins, 1–60% B; 2–6 mins 60–85% B; 6–8 mins 85–99% B; 8–10 mins 99–1% B. Features were measured in both positive and negative electrospray ionization modes with the following mass spectrometer parameters: capillary voltage, 2kV; cone voltage, 40V; source temperature, 150°C; desolvation gas flow and temperature, 1200L h^{-1} and 600°C; cone gas flow, 50L h^{-1} . Data was acquired in centroid, using the MS^E method in resolution mode. The MS^E method generates both the precursor ion (function 1) and fragment ions (function 2) in one acquisition. The acquisition period was 11 minutes, with a 0.05 second scan time and a mass range of 50 – 1200 Da. Collision energy was set to 0 V for function 1 and was ramped from 15 – 50 V for function 2. Leucine-enkephalin (0.9 μM) was used as lockspray solution to ensure mass accuracy. The lockspray solution was infused at a flow rate of 10 $\mu\text{L mL}^{-1}$. Lockmass was acquired at intervals of 10 seconds and averaged over 3 scans.

2.6 Data processing

Data processing was performed using the R statistical programming language. Waters raw data files generated from the metabolomics analysis were converted to mzData files using the `convert.waters.raw` R package. The quality control pooled injections were used to find the optimal peak picking parameters, retention time corrections and grouping parameters with the isotopologue parameter optimization (IPO) package. The resulting parameters were inputted into the XCMS package for peak-picking, to integrate the area under the curve and to replace zero values. The CAMERA package was applied to XCMS processed features to annotate possible isotopes and adducts. XCMS and CAMERA packages were used to combine data from both positive and negative ionization modes. The resulting data was subsequently normalized to internal standards, and features were filtered by applying a threshold of 30% relative standard deviation within quality control injections. Urinary metabolites were normalized to both urinary creatinine and internal standards, to account for differences in urine concentration. Features were grouped by retention time and correlation into “pcgroups” by the CAMERA package. Within each pcgroup, only the feature with the highest mean raw intensity was kept for further data analysis.

2.7 Data and Statistical Analysis

The raw intensity values of all features were log transformed using MetaboAnalyst 5.0, to remove heteroscedasticity and correct for skewed data distribution. Any 0 values during log transformation were treated as 1/5 of the minimum intensity values of each feature. Log transformed feature intensity values were used for all analysis unless stated otherwise.

The EZInfo 2.0 software (Umetrics, Umeå, Sweden) was used to perform multivariate analysis on the metabolomics data. Data was centered and pareto scaled upon import into EZInfo 2.0. Principal component analysis (PCA) was used to visualize unsupervised metabolic variation between saline and cisplatin treatment at each of the timepoints of the study. Orthogonal partial least squares discriminant analysis (OPLS-DA), a supervised discriminatory analysis, was used for the pairwise discrimination of treatment groups at each timepoint. For each OPLS-DA, metabolites were ranked by their correlation ($p(\text{corr})$) values and variable importance in projection (VIP) values to select a subset of metabolites for identification. Features with $0.4 < p(\text{corr}) < -0.4$ and $\text{VIP} > 1$ were considered as important discriminators of the groups being compared.

Features were analyzed by two-way ANOVA with Benjamini-Hochberg false discovery rate (FDR) correction to find features that were significantly different by saline vs. cisplatin treatment. The DEGreport (1.30.3) R package was used to generate hierarchical clusters of features that were determined by two-way ANOVA as being significantly altered by treatment. The Z-scores presented in these time course figures (**Figure**

5) are calculated by centering each feature to its mean and dividing by the standard deviation of the feature. Clusters were selected for further analysis based on time course patterns of clinical interest, focusing on features that are differently expressed in the early timepoints (day 1 and 2) between the saline and cisplatin-treated mice. Individual features that were found to be significantly different by two-way ANOVA and FDR correction were further analyzed by pairwise t-tests comparing saline vs. cisplatin treated mice at each timepoint, with p-values adjusted for multiple comparisons using Bonferroni correction. $p < 0.05$ was considered as significantly significant for all univariate data analysis.

Univariate and multivariate receiver operating characteristic (ROC) curves were generated using MetaboAnalyst 5.0. Multivariate ROCs were generated using linear support vector machine classification, with features ranked by highest to lowest univariate area under the ROC (AUROC) values.

2.8 Putative metabolite identification

The m/z and fragmentation spectra of features were cross referenced with online metabolite databases Human Metabolome Database (HMDB), METLIN, or MassBank for putative metabolite annotation. Analytical standards were purchased and analyzed in parallel with biological samples to achieve a level 1 identification

3. RESULTS

3.1 Assessment of renal injury

The extent of injury caused by cisplatin treatment was assessed in both mouse strains by plasma creatinine levels (**Figure 1A and 1C**) and histological evaluation by a clinical pathologist (**Figure 1B and 1D**). Plasma creatinine concentrations were 4.3-fold and 5.4-fold higher in day 4 cisplatin-treated C57BL/6 and FVB/N mice, respectively, compared to day 4 saline controls ($p < 0.05$). In day 3 cisplatin-treated C57BL/6 and FVB/N mice, plasma creatinine concentrations were increased 2.3-fold and 2.0-fold compared to saline controls, although this difference was not statistically significant. In day 3 cisplatin-treated mice, 3/9 (33%) C57BL/6 mice and 5/8 (62.5%) FVB/N mice showed signs of histological renal injury (injury score [?] 1), whereas on day 4, histological damage was observed in 6/8 (75%) and 5/7 (71.4%) cisplatin-treated C57BL/6 and FVB/N mice, respectively. Histological injury was not observed at any other timepoint, with the exception of one C57BL/6 mouse in the day 1 cisplatin group (1/9, 11.1%).

3.2 Metabolomic profiling of saline-treated vs. cisplatin-treated mice over time

XCMS processing of chromatographic data and subsequent filtering by relative standard deviation of features in pooled quality control samples resulted in the selection of 2446 features for plasma, 2319 features for urine, and 3021 features for kidney. Following pcgroup filtering (as described in the methods section), 841 plasma features, 999 urine features, and 841 kidney features remained for analysis.

PCA score plots were generated to visualize the metabolic variation between saline-treated mice and cisplatin-treated mice at each of the four timepoints. Score plots of plasma, urine, and kidney samples from C57BL/6 mice all showed a clear separation between saline and cisplatin groups from days 2-4 (**Figure S1**), with moderate separation observed at day 1 for all three sample types (**Figure S1**). Similar trends were observed in PCA score plots of FVB/N mice, with clear separation between saline and cisplatin-treated mice from day 2-4 for all sample types and weak to moderate separation at day 1 (**Figure S2**). Corresponding OPLS-DA models of pairwise comparisons between saline and cisplatin-treated mice at each timepoint confirmed the separation observed in PCA scores plots, with a high degree of fit (R^2Y) and moderate predictive ability (Q^2Y) between days 2-4 for both C57BL/6 (**Figure 2**) and FVB/N mice (**Figure S3**). OPLS-DA models of day 1 plasma samples for both strains of mice showed good fit and moderate predictive ability, but model statistics were poor for day 1 urine and kidney samples (**Figure 2, S3**).

In C57BL/6 mice, two-way ANOVA of individual features for each sample type revealed 181 plasma features, 683 urine features, and 66 kidney features that were significantly different by saline vs. cisplatin treatment after adjusting for multiple comparisons. Significant differences were found in 109 plasma features, 599 urine

features, and 73 kidney features when comparing samples from saline and cisplatin-treated FVB/N mice. Within each sample type, significant features following similar time course patterns were grouped together by using hierarchical clustering, and clusters containing features showing early alterations were selected for further analysis (C57BL/6, **Figure 3** ; FVB/N, **Figure S4**). To further narrow down important features, pairwise t-tests were performed between saline and cisplatin groups at each timepoint for each individual feature. Features that were significantly different in the early timepoints (day 1 or day 2) for either strain were selected for identification, summarized in **Table 1** (C57BL/6) and **Table 2** (FVB/N).

3.3 Early plasma biomarkers of cisplatin-induced acute kidney injury

The majority of plasma metabolites (130/181, 71.8%) were decreased by cisplatin treatment in C57BL/6 mice (**Figure 3A**). Plasma creatine, L-acetylcarnitine, p-cresol sulfate, phenylalanine, taurine, sulfolithocholyglycine, taurocholate, and tryptophan were among identified plasma metabolites that were increased by cisplatin treatment (**Figure 4**, **S5**). In C57BL/6 mice, L-acetylcarnitine and taurine were significantly increased as early as day 1 and day 2, respectively, and remained elevated throughout day 3 and 4 (**Figure 4C**, **4H**). Although L-acetylcarnitine and taurine were also elevated with cisplatin treatment in FVB/N mice, these changes were only significant on days 3 and 4 (**Figure S5C**, **S5H**). Amino acids phenylalanine and tryptophan exhibited early increases in both strains, though C57BL/6 mice showed significant changes earlier than FVB/N mice. Phenylalanine and tryptophan were significantly elevated on day 1 after cisplatin treatment in C57BL/6 mice (**Figure 4F**, **4J**), whereas significant increases in both amino acids were observed two days following cisplatin treatment in FVB/N mice (**Figure S5F**, **S5J**). Bile acids sulfolithocholyglycine and taurocholic acid showed a similar pattern for both strains of mice, where a transient but significant elevation was observed on day 2 for C57BL/6 mice (**Figure 4G**, **4I**) and days 2 and 3 for FVB/N mice (**Figure S5G**, **S5I**). Creatine and p-cresol sulfate were significantly elevated in cisplatin-treated FVB/N mice from days 2-4 (**Figure S5A**, **S5E**), and although they showed the same pattern of elevation in C57BL/6 mice, the changes were not statistically significant (**Figure 4A**, **4E**).

2,3-dihydroxybenzoic acid, equol 4-sulfate, and LysoPC(20:3) were among plasma metabolites decreased by cisplatin treatment (**Figure 4**, **S5**). In C57BL/6 mice, 2,3-dihydroxybenzoic acid decreased in the early timepoints, but did not show significant early alterations in the plasma of FVB/N mice. Plasma LysoPC(20:3) was consistently decreased for all timepoints for C57BL/6 mice but was not significantly changed in FVB/N mice until day 3. Lastly, plasma levels of equol 4-sulfate were significantly lower in FVB/N mice from days 2-4, but no significant changes were observed in C57BL/6 plasma until day 4 (**Figure S5**).

3.4 Early urine biomarkers of cisplatin-induced acute kidney injury

The vast majority of urinary metabolites were decreased following cisplatin treatment. Of 683 metabolites significantly altered by cisplatin treatment in C57BL/6 mice, 665 were decreased (97.3%, **Figure 3B**), whereas 550/599 (91.8%) metabolites were decreased in FVB/N mice (**Figure S4B**). Out of the identified metabolites, L-carnitine was the only metabolite increased by cisplatin treatment (**Figure 5G**, **S6G**), and was consistently elevated in the urine of C57BL/6 mice from day 2-4 (**Figure 5G**). In FVB/N mice, L-carnitine was also higher in the urine of cisplatin-treated mice throughout all timepoints, though only significant on day 1 (**Figure S6G**).

Citric acid, equol, equol 7-O-glucuronide, homovanillic acid sulfate, indole-3-carboxaldehyde, indole-3-carboxylic acid, phenylpropionylglycine, pyrocatechol sulfate, succinate, trigonelline, and tyrosol 4-sulfate were all significantly decreased by cisplatin treatment. In both strains of mice, equol, equol 7-O-glucuronide, indole-3-carboxaldehyde, succinate, and trigonelline were all significantly lower in the cisplatin groups from days 2-4 (**Figure 5**, **S6**). Citric acid, homovanillic acid sulfate, indole-3-carboxylic acid, phenylpropionylglycine, pyrocatechol sulfate, and tyrosol 4-sulfate showed a similar pattern, with decreased levels of these metabolites in cisplatin treated mice from days 2-4, albeit not achieving significance at all time points for both strains (**Figure 5**, **S6**).

3.5 Early kidney biomarkers of cisplatin-induced acute kidney injury

Hierarchical clustering revealed that the majority of significantly altered kidney metabolites were increased by cisplatin treatment, with 44/63 (69.8%) of metabolites being increased in C57BL/6 mice (**Figure 3C**) and 50/73 (68.5%) metabolites increased in FVB/N mice (**Figure S4C**). Creatine, p-cresol glucuronide, p-cresol sulfate, phenylacetylglycine, phenylalanine, and tryptophan were found to be elevated by cisplatin treatment in kidney tissue. Creatine showed significant elevation throughout all four timepoints in FVB/N mice, and similarly was also increased in C57BL/6 mice, though only significantly increased at days 2 and 3 (**Figure 6A, S7A**). P-cresol glucuronide (**Figure S7D**), p-cresol sulfate (**Figure S7E**), and phenylacetylglycine (**Figure S7F**) were all significantly elevated from day 2-4 in cisplatin-treated FVB/N kidneys. These metabolites followed a similar pattern in C57BL/6 mice but were significantly altered only at day 3 and 4 for p-cresol glucuronide and sulfate (**Figure 6D, 6E**), and days 1 and 4 for phenylacetylglycine (**Figure 6F**). Kidney levels of phenylalanine (**Figure 6G, S7G**) and tryptophan (**Figure 6J, S7J**) were also generally increased by cisplatin treatment, but only tryptophan in C57BL/6 mice was shown to be significantly increased in the early timepoints (**Figure 6J**).

Equol 4-sulfate, LysoPC(20:3), proline betaine, and trigonelline were kidney metabolites identified to be decreased by cisplatin treatment. In kidneys from FVB/N mice, levels of equol 4-sulfate were significantly decreased following cisplatin treatment for all timepoints (**Figure S7B**), and though equol 4-sulfate followed this decreasing trend in C57BL/6 kidneys, none of the changes were significant (**Figure S7B**). Proline betaine was consistently altered by cisplatin treatment in both strains, being significantly decreased from days 2-4 (**Figure 6H, S7H**). LysoPC(20:3) and trigonelline were also significantly decreased from days 2-4 in cisplatin-treated FVB/N mice (**Figure S7C, S7I**). These metabolites exhibited similar trends in C57BL/6 kidneys, though they were only significantly altered on day 4 for both metabolites (**Figure 6C, 6I**).

3.6 Assessment of the diagnostic performance of biomarkers

Univariate ROC curves were generated for each metabolite at each timepoint, and univariate AUROC was calculated to assess the diagnostic performance of each individual metabolite. All AUROC values for early plasma markers were summarized in **Figure 7A** for C57BL/6 mice and **Figure S8A** for FVB/N mice. All AUROC values for early urine markers were summarized in **Figure 8A** for C57BL/6 mice and **Figure S9A** for FVB/N mice. Metabolites were ranked from highest to lowest univariate AUROC values. Multivariate ROCs were generated to assess the aggregate diagnostic performance of a combination of metabolites, ranging from a combination of the top two highest ranked metabolites to the top 10 and top 15 ranked metabolites for plasma (**Figure 7, S8**) and urine (**Figure 8, S9**), respectively.

An AUROC value [?] 0.7 is generally considered to be acceptable. When discriminating saline vs. cisplatin treated C57BL/6 mice, plasma creatinine had an AUROC of 0.719 at day 1. Nine plasma metabolites had an AUROC [?] 0.7 when discriminating saline vs. cisplatin-treated C57BL/6 mice on day 1 (creatine; 0.729, equol 4-sulfate; 0.736, L-acetylcarnitine; 0.944, L-carnitine; 0.944, LysoPC(20:3); 0.875, phenylalanine; 0.917, taurocholic acid; 0.708, trigonelline; 0.785, and tryptophan; 0.826). Eight of the nine metabolites with AUROC [?] 0.7 on day 1 outperformed plasma creatinine, with the exception of taurocholic acid. In FVB/N mice, plasma creatinine had an AUROC of 0.562 at day 1. Five plasma metabolites in FVB/N mice had an AUROC [?] 0.7 at day 1 (creatine; 0.773, pyrocatechol sulfate; 0.828, taurine; 0.719, taurocholic acid; 0.891, and trigonelline; 0.891). All 5 metabolites with AUROC [?] 0.7 on day 1 outperformed plasma creatinine on day 1.

Multivariate ROCs generated for C57BL/6 plasma samples at day 1 revealed a maximum AUROC of 0.877, which was achieved in the ROC curve modeled using the top three ranked metabolites: L-acetylcarnitine, phenylalanine, and LysoPC(20:3) (**Figure 7B**). The maximum multivariate AUROC achieved in C57BL/6 urine was 0.545 on day 1, but reached AUROC values of 1 in all combinations of the top two to top 15 metabolites on day 2 (**Figure 8B, 8C**). In FVB/N plasma, a peak AUROC of 0.656 was obtained at day 1, whereas AUROC values of [?] 0.991 were observed on day 2 for all combinations of metabolites (**Figure S8B, S8C**). In day 1 FVB/N urine samples, the highest multivariate AUROC value of 0.940 was produced via the combination of all 15 early urine metabolites (**Figure S9B**). Diagnostic performance was further

improved in day 2 FVB/N urine, with all metabolite combinations yielding an AUROC [?] 0.953 (**Figure S9C**).

4. DISCUSSION

In this study, untargeted metabolomics was employed in a mouse model of cisplatin-induced AKI to investigate early metabolic changes following cisplatin administration. Previous studies have utilized untargeted metabolomics to study rodent models of cisplatin-induced AKI, but have typically focused on studying one or two biological matrices. Furthermore, though some of these studies have looked at the metabolic alterations induced by cisplatin-induced AKI over multiple timepoints, others have only studied a single timepoint after establishment of AKI. To our knowledge, our study is the first to comprehensively assess temporal metabolic alterations in all three of plasma, urine, and kidney samples throughout AKI progression. Additionally, our study used two separate strains of mice, allowing for the corroboration of metabolic changes observed in either strain. Metabolites that exhibited early alterations in plasma, urine, and kidney samples were identified as potential early biomarkers for cisplatin-induced nephrotoxicity; in total, 26 such metabolites were identified.

The extent of renal injury throughout the day 1-4 timepoints was assessed by plasma creatinine and histological assessment. Similar to cisplatin nephrotoxicity in humans, AKI only manifested in the later timepoints, and kidney injury was not apparent in all cisplatin treated mice. Previous studies have reported that FVB/N mice are more sensitive to cisplatin-induced AKI compared to C57BL/6 mice, but surprisingly, there was no difference between the two strains in this study. This lack of difference in cisplatin sensitivity may be due to the relatively mild injury observed. This is likely a result of using a cisplatin dose on the lower end of the established 10-30 mg kg⁻¹ range for mouse models.

Mitochondrial dysfunction is a key component of the pathogenesis of AKI, with the kidneys being an organ with very high energy demand. Many metabolites identified as early biomarkers were related to mitochondrial energy metabolism, including metabolites related to fatty acid β -oxidation (FAO) and the tricarboxylic acid (TCA) cycle. Cisplatin has previously been shown to inhibit FAO by deactivating PPAR- α , a nuclear receptor that plays a crucial role in the regulation of FAO. L-carnitine plays a vital role in FAO, allowing for the transport of long chain fatty acids across the mitochondrial inner membrane. Plasma accumulation of acylcarnitines, formed by the conjugation of L-carnitine and fatty acids, are indicative of disorders FAO. Both L-carnitine and L-acetylcarnitine were altered by cisplatin treatment, with early elevations observed for urinary L-carnitine in both mouse strains and early increases in plasma L-acetylcarnitine levels in C57BL/6 mice. These cisplatin-induced alterations in urinary L-carnitine and plasma L-acetylcarnitine were sustained throughout the duration of the study. L-carnitine and acylcarnitines have previously been shown to be altered in other rodent models of cisplatin-induced nephrotoxicity and human patients undergoing cisplatin chemotherapy. In patients receiving cisplatin, urinary excretion of L-carnitine was significantly increased even on the first day of cisplatin treatment, with increased urine levels being maintained for the next two days. Though studies have shown accumulation of acylcarnitines in the blood as early as 24 hours following cisplatin administration, our study is the first metabolomics study to show an early elevation of plasma L-acetylcarnitine, specifically, following cisplatin administration. In addition to markers of dysfunctional FAO, 15urine levels of TCA cycle intermediates citric acid and succinate showed significant decreases as early as two days after cisplatin treatment in C57BL/6 mice, in accordance with previous studies linking cisplatin and early alterations of TCA cycle intermediates in urine. Moreover, creatine, which plays a crucial role in the creatine kinase-phosphocreatine circuit, was consistently increased in the plasma, urine, and kidneys of both strains of mice throughout progression of kidney damage, though alterations were more pronounced in FVB/N mice. The creatine kinase system is responsible for coupling cellular sites of ATP production to sites of ATP consumption and is particularly sensitive to oxidative stress. An overall accumulation of creatine suggests an impairment in the generation of high energy phosphate molecules.

Gut-derived metabolites of tryptophan indole-3-carboxaldehyde and indole-3-carboxylic acid were found to be significantly decreased as early as day 1 and day 2, respectively, in the urine of cisplatin-treated mice. Both indole-3-carboxaldehyde and indole-3-carboxylic acid have shown the ability to activate aryl

hydrocarbon receptor (AhR) , which has been shown to induce renal fibrosis, podocyte injury, glomerular damage, inflammation, and is correlated with exacerbation of chronic kidney disease in both animal models and human patients . Phenylalanine and downstream gut-derived metabolites of phenylalanine also exhibited early alterations following cisplatin treatment in our study. Phenylalanine was elevated in plasma, urine, and kidney samples following cisplatin exposure, with plasma levels being significantly elevated as early as day 1 in C57BL/6 mice and day 2 in FVB/N mice. Phenylalanine is metabolized by intestinal bacteria to p-cresol , which is subsequently metabolized to p-cresol sulfate or p-cresol glucuronide in the liver . Both p-cresol conjugates were elevated in plasma, urine, and kidneys with cisplatin treatment, where the most striking and consistent differences were observed in FVB/N mice. P-cresol derivatives have predominantly been studied in the setting of chronic kidney disease, where they have been associated with exacerbation of renal injury and cardiovascular disease . Additionally, urinary excretion of acylglycines phenylpropionylglycine and phenylacetyl-glycine, gut-derived down-stream metabolites of phenylalanine , were found to be altered in cisplatin-treated mice. Urinary excretion of phenylpropionylglycine was consistently decreased in both mouse strains throughout cisplatin treatment, whereas phenylacetyl-glycine was shown to accumulate in the kidneys, altogether suggesting tissue accumulation of acylglycine compounds. Acylglycines have historically been used as markers of disorder of metabolism and FAO, where a defect in β -oxidation is typically characterized by an increased urinary excretion of acylglycines . An accumulation of intracellular acyl-CoA due to disorders of FAO is associated with toxicity and detrimental to mitochondrial function , and conjugation of glycine with these acyl-CoA compounds to form acylglycines has shown to have a detoxification effect .

Metabolomics analysis also revealed dietary metabolites to be affected by cisplatin treatment. In both strains of mice, urinary excretion of dietary phenolic metabolites homovanillic acid sulfate, pyrocatechol sulfate, and tyrosol 4-sulfate were significantly decreased two days after cisplatin treatment and remained decreased throughout the study. Metabolomics studies in CKD rats and CKD patients have also reported the accumulation of plasma pyrocatechol sulfate in the setting of renal decline . Polyphenolic compounds found in olive oil, including unconjugated precursors of homovanillic acid sulfate and tyrosol 4-sulfate (homovanillic acid and tyrosol, respectively) have routinely been reported to possess a multitude of health benefits in a variety of pathophysiological conditions . Trigonelline is a dietary plant alkaloid that has been reported to possess hypoglycemic, anti-diabetic, antioxidant and overall renoprotective properties. Trigonelline was consistently reduced in the urine and kidneys of cisplatin treated mice. Studies have shown trigonelline to have beneficial effects against diabetic nephropathy , and in attenuating epithelial-to-mesenchymal transition and ROS generation in an oxalate-induced *in vitro* model of renal fibrosis . Our study adds to previous findings from a metabolomics study in a mouse model of cisplatin-induced AKI which reported an early decrease in urinary trigonelline , by showing decreased levels of trigonelline in the plasma and kidneys of cisplatin-treated mice in addition to urine.

Taurine is a β -amino acid that has a protective role against oxidative stress, reducing mitochondrial production of oxidants . Additionally, taurine plays a crucial role in post-translation modification of mitochondrial tRNAs, which are important in leucine and lysine synthesis, and by extension mitochondrial protein translation of electron transport chain complexes . In our study, taurine was significantly higher in the plasma of day 2 cisplatin treated C57BL/6 mice, though a significant elevation was not observed until day 3 in the plasma of FVB/N mice. Taurine enters tubular cells via uptake by taurine transporter (TauT). TauT is found on both apical and basolateral membranes of renal tubular cells, with expression varying based on tubular cell type . Cisplatin exposure to proximal tubule cells for 24 hours *in vitro* has been shown to downregulate gene and protein expression of TauT and reduce the function of TauT, potentially through stimulation of p53 . Alterations in taurine transport may help to explain the plasma accumulation of taurine observed in our study.

As previously discussed, the main strength of our study was the comprehensive metabolomic analysis of three biological matrices sampled at multiple timepoints throughout the progression of kidney injury. Moreover, two separate strains of mice were investigated, demonstrating that cisplatin-induced metabolic alterations could be reproduced in two different strains of mice. There were also some limitations to this study. Firstly, only male mice were studied, and sex differences could not be assessed. Additionally, diet is known to affect

metabolomics; mice had free access to chow *ad libitum*, and cisplatin-treated mice were observed to eat less compared to saline controls.

5. CONCLUSION

Current clinical markers of AKI are incapable of detecting cisplatin-induced nephrotoxicity prior to the establishment of significant renal injury and functional impairment, and there is a need for biomarkers that are capable of earlier detection. In this study, a total of 26 plasma, urine, and kidney metabolites were identified as potential early biomarkers of cisplatin-induced acute kidney injury. Alterations in these metabolites over time following cisplatin administration were consistent in two separate strains of mice. These markers may help to better understand the pathophysiological mechanisms behind cisplatin nephrotoxicity and AKI in general. Many of these metabolites are indicative of dysregulated mitochondrial dysfunction, highlighting the detrimental effects of cisplatin on mitochondria. Many metabolites were dietary and gut-derived, indicating the need to investigate the crosstalk between the gut and the kidney in the setting of acute kidney injury. Our study provides a large panel of metabolites that can be targeted for future clinical studies of early detection of AKI and may provide guidance in the selection of therapeutic targets against cisplatin-induced nephrotoxicity. Further studies are necessary to validate the applicability, utility, and translatability of these metabolites in a clinical setting.

DATA AVAILABILITY STATEMENT

Data collected in this study are available upon request from the corresponding author Bradley L. Urquhart.

FUNDING STATEMENT

This study was funded by project grants from the Canadian Institutes of Health Research and Canada Foundation for Innovation.

AUTHOR CONTRIBUTION STATEMENT

B.L.U. and Y.J.L. designed the study. Y.J.L. performed the research and data analysis. E.D.H. and N.C.T. assisted with animal work. T.J.V. provided guidance with data analysis. A.H. developed and implemented kidney injury scoring and analysis. Y.J.L. drafted the manuscript. B.L.U. edited the manuscript for final submission. All authors have reviewed and approved the submitted manuscript.

CONFLICT OF INTEREST DISCLOSURE

The authors declare no conflicts of interest.

ORCID

Bradley L. Urquhart: 0000-0001-8324-1472

REFERENCES

FIGURE LEGENDS

Figure 1. Assessment of renal injury in untreated (black), saline-treated (blue), and cisplatin-treated (red) C57BL/6 mice (**A, B**), and FVB/N mice (**C, D**). Plasma creatinine concentrations (**A, C**) were normalized to creatinine-d3 standard before quantification. (**B, D**) H&E-stained kidney sections were scored from 0-5 based on severity of renal injury by a pathologist blinded to treatment conditions. n=5-9 (exact sample sizes can be found in **Table S1**), error bars represent mean \pm SD. Statistical analysis was performed using two-way ANOVA, *p < 0.05 compared to saline control.

Figure 2. Orthogonal partial least squares discriminant analysis scores plots comparing plasma (**A-D**), urine (**E-H**), and kidney (**I-L**) samples from saline-treated (black) and cisplatin-treated (red) C57BL/6 mice at each timepoint: day 1 (**A, E, I**), day 2 (**B, F, J**), day 3 (**C, G, K**), day 4 (**D, H, L**). Model statistics for OPLS-DA were as follows: (**A**) $R^2Y = 0.989$, $Q^2Y = 0.369$ (**B**) $R^2Y = 0.980$, $Q^2Y = 0.542$ (**C**) $R^2Y = 0.989$, $Q^2Y = 0.467$ (**D**) $R^2Y = 0.985$, $Q^2Y = 0.580$ (**E**) $R^2Y = 0.627$, $Q^2Y = 0.033$ (**F**) R^2Y

= 0.989, $Q^2Y = 0.649$ (**G**) $R^2Y = 0.989$, $Q^2Y = 0.295$ (**H**) $R^2Y = 0.946$, $Q^2Y = 0.581$ (**I**) $R^2Y = 0.914$, $Q^2Y = 0.101$ (**J**) $R^2Y = 0.979$, $Q^2Y = 0.611$ (**K**) $R^2Y = 0.944$, $Q^2Y = 0.426$ (**L**) $R^2Y = 0.973$, $Q^2Y = 0.569$. n=5-10, exact sample sizes can be found in **Table S1** .

Figure 3. Time course cluster analysis of (A) plasma, (B) urine, and (C) kidney features that were significantly altered by cisplatin treatment in C57BL/6 mice. The lighter, thinner lines represent change over time for each individual feature within each cluster, and the darker, thicker line represents the mean z-score for all features in each cluster. Boxes represent the median and interquartile range (IQR), and the whiskers represent 1.5x IQR.

Figure 4. Log transformed relative intensity of features significantly affected by cisplatin treatment in plasma samples from C57BL/6 mice. Data are presented as box and whisker plots, where boxes represent the median and interquartile range (IQR), and whiskers represent 1.5x IQR. Statistical analysis was performed using two-way ANOVA, * $p < 0.05$ compared to saline control at each timepoint. n=5-9, exact sample sizes can be found in **Table S1** .

Figure 5. Log transformed relative intensity of features significantly affected by cisplatin treatment in urine samples from C57BL/6 mice. Data are presented as box and whisker plots, where boxes represent the median and interquartile range (IQR), and whiskers represent 1.5x IQR. Statistical analysis was performed using two-way ANOVA, * $p < 0.05$ compared to saline control at each timepoint. n=6-9, exact sample sizes can be found in **Table S1** .

Figure 6. Log transformed relative intensity of features significantly affected by cisplatin treatment in kidney samples from C57BL/6 mice. Data are presented as box and whisker plots, where boxes represent the median and interquartile range (IQR), and whiskers represent 1.5x IQR. Statistical analysis was performed using two-way ANOVA, * $p < 0.05$ compared to saline control at each timepoint. n=7-10, exact sample sizes can be found in **Table S1** .

Figure 7. Receiver operating characteristic (ROC) analysis of early plasma biomarkers. (**A**) Summary of area under the ROC curve values calculated for each plasma metabolite at all timepoints. (**B, C**) Multivariate ROC curves generated at (**B**) day 1 and (**C**) day 2 using a variable number of metabolites. ROC curves were generated using a sequential combination of the top two to top ten ranked metabolites, where each metabolite was ranked using the calculated univariate AUROC at each respective timepoint.

Figure 8. Receiver operating characteristic (ROC) analysis of early urine biomarkers in C57BL/6 mice. (**A**) Summary of area under the ROC curve values calculated for each urine metabolite at all timepoints. (**B, C**) Multivariate ROC curves generated at (**B**) day 1 and (**C**) day 2 using a variable number of metabolites. ROC curves were generated using a sequential combination of the top two to top 15 ranked metabolites, where each metabolite was ranked using the calculated univariate AUROC at each respective timepoint.

FIGURE 1

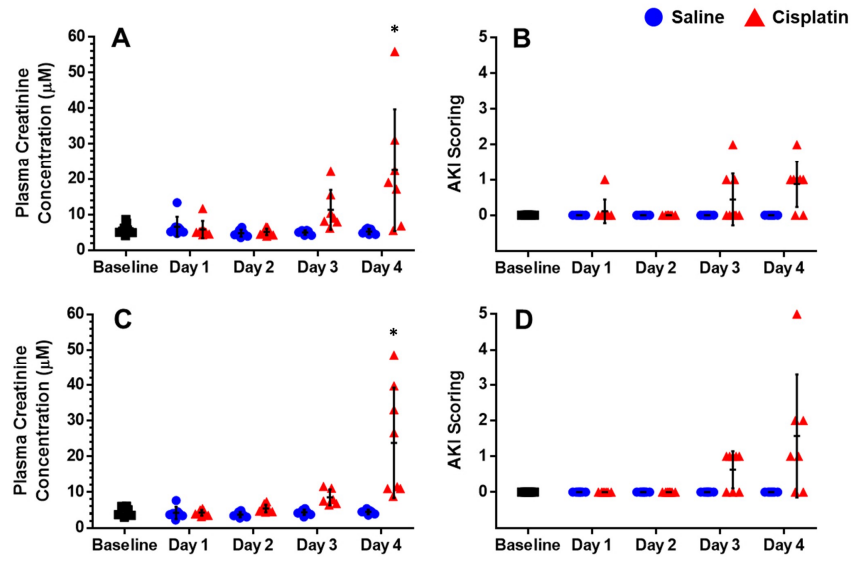


FIGURE 2

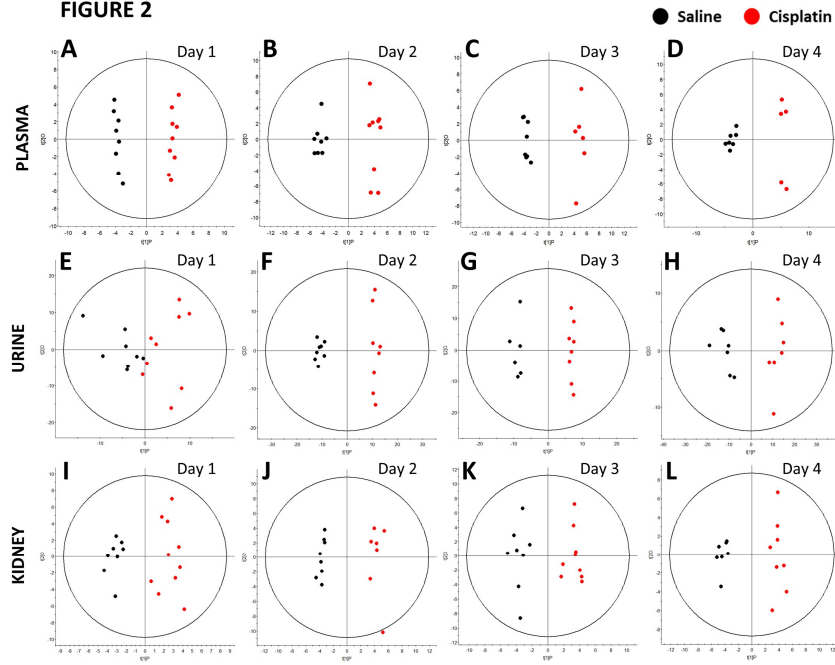
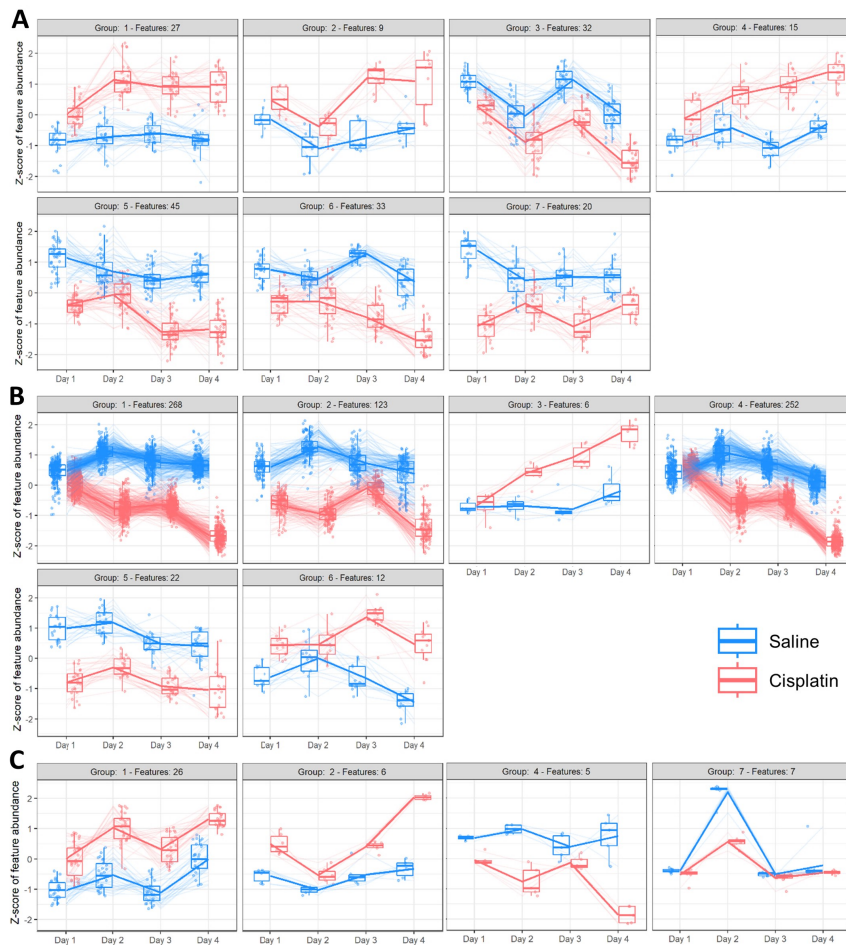
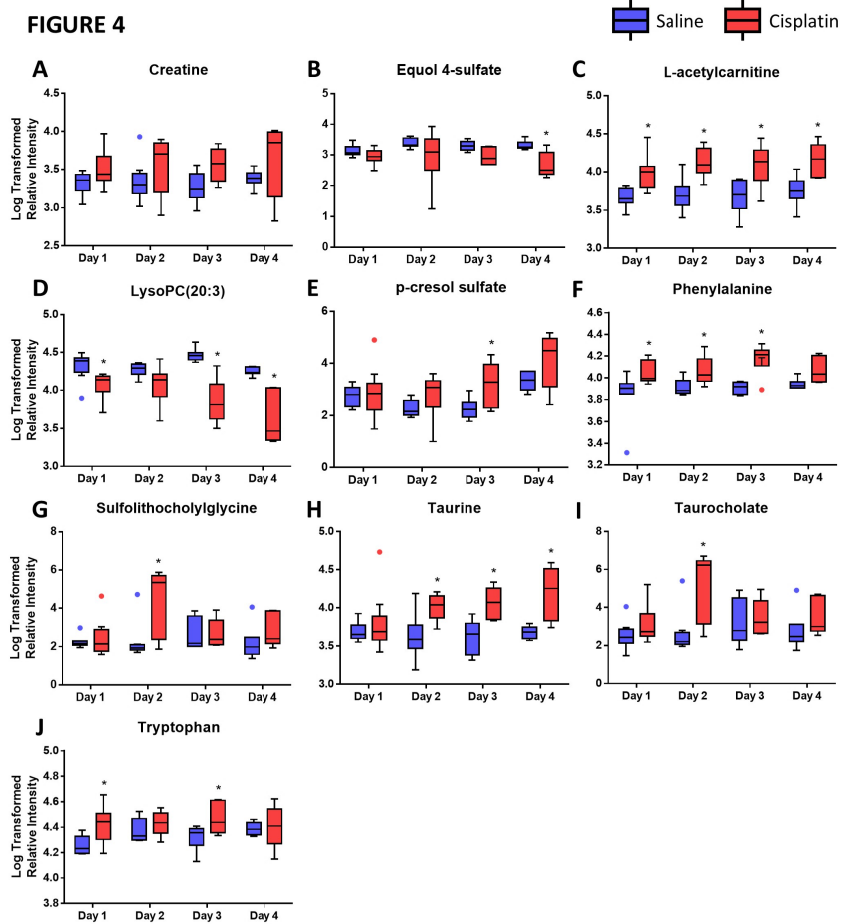
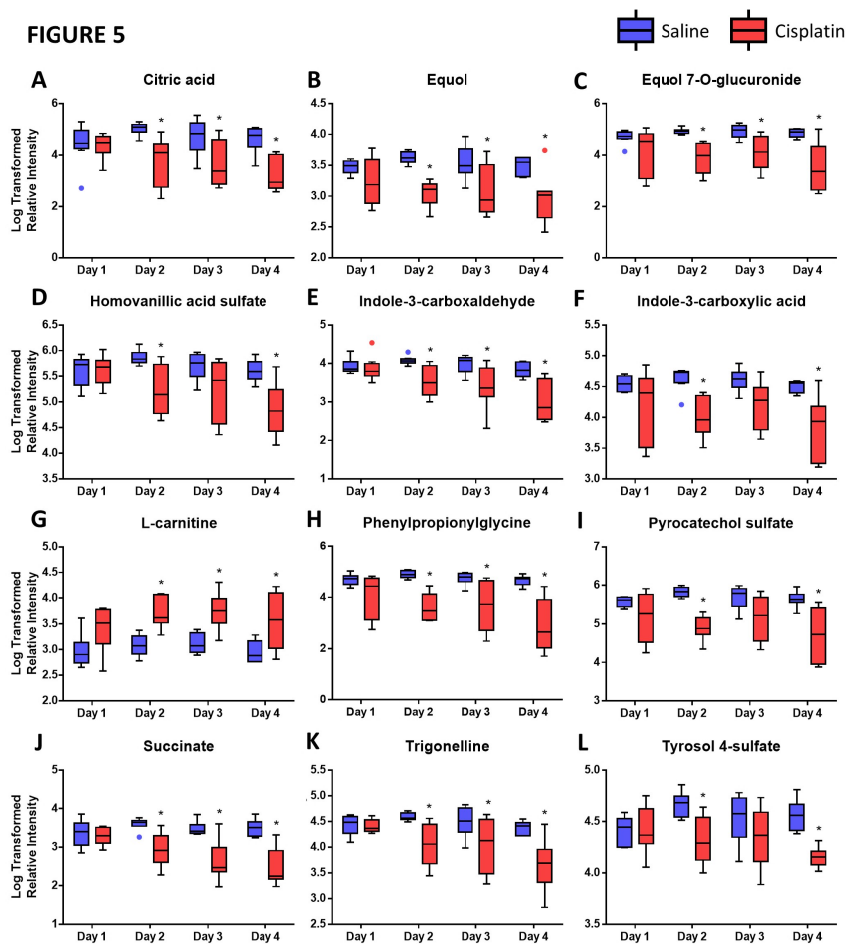


FIGURE 3







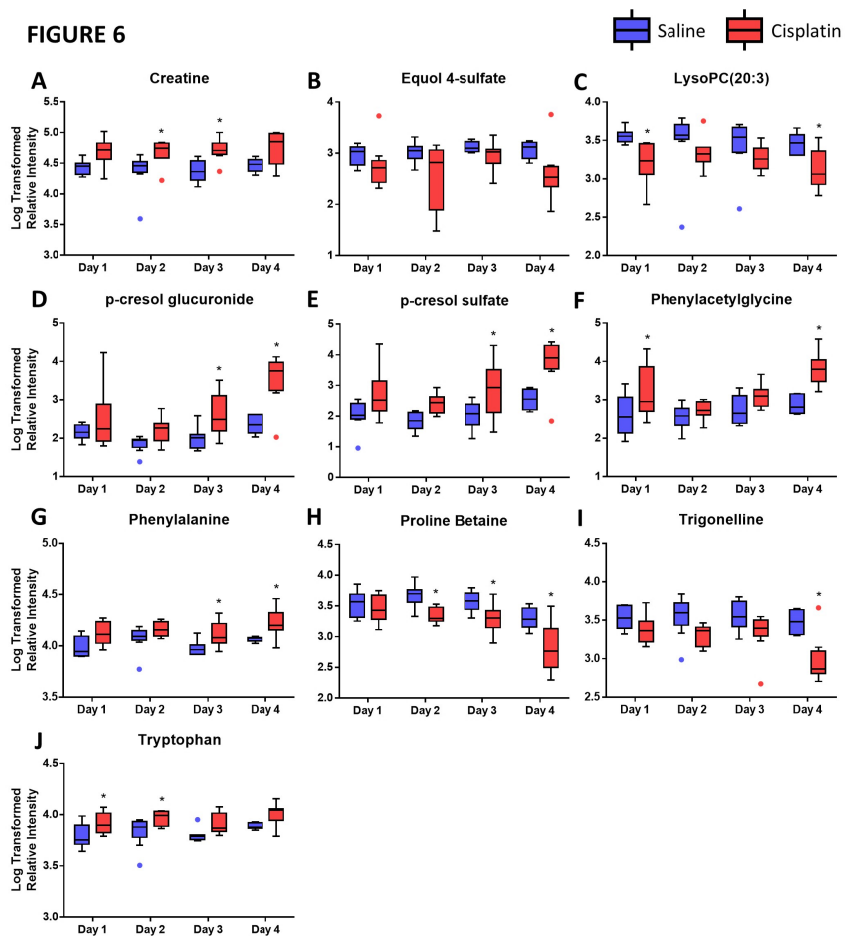


FIGURE 7

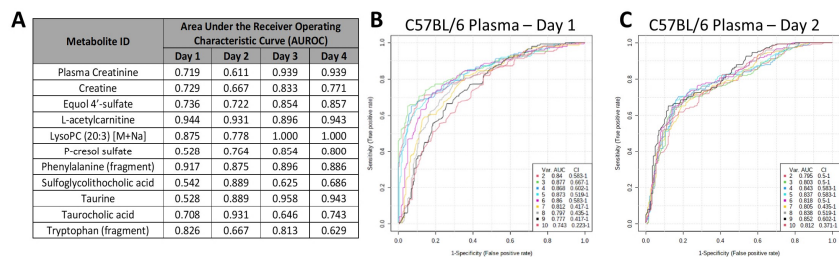
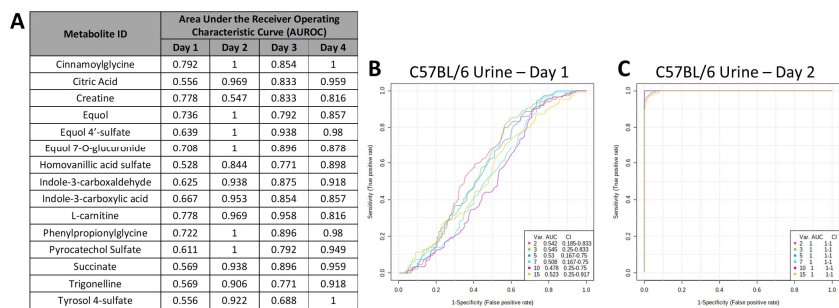


FIGURE 8



Hosted file

Table 1.docx available at <https://authorea.com/users/507657/articles/607535-metabolomics-for-the-identification-of-early-biomarkers-of-cisplatin-induced-nephrotoxicity-in-a-mouse-model-of-cisplatin-induced-acute-kidney-injury>

Hosted file

Table 2.docx available at <https://authorea.com/users/507657/articles/607535-metabolomics-for-the-identification-of-early-biomarkers-of-cisplatin-induced-nephrotoxicity-in-a-mouse-model-of-cisplatin-induced-acute-kidney-injury>